Friedel-Like Oscillations from Interstitial Iron in Superconducting $Fe_{1+y}Te_{0.62}Se_{0.38}$

V. Thampy,[1] J. Kang,[1] J. A. Rodriguez-Rivera,[2,3] W. Bao,[4] A. T. Savici,[5] J. Hu,[6] T. J. Liu,[6] B. Qian,[6] D. Fobes,[6] Z. Q. Mao,[6] C. B. Fu,[7,8,9] W. C. Chen,[3,9] Q. Ye,[5] R. W. Erwin,[2] T. R. Gentile,[9] Z. Tesanovic,[1] and C. Broholm[1,2]

[1]*Institute for Quantum Matter and Department of Physics and Astronomy, Johns Hopkins University, Baltimore, Maryland 21218, USA*
[2]*NIST Center for Neutron Research, National Institute of Standards and Technology, Gaithersburg, Maryland 20899, USA*
[3]*Department of Materials Science and Engineering, University of Maryland, College Park, Maryland 20740, USA*
[4]*Department of Physics, Renmin University of China, Beijing 100872, China*
[5]*NSSD, Oak Ridge National Laboratory, Oak Ridge, Tennessee 37831, USA*
[6]*Department of Physics, Tulane University, New Orleans, Louisiana 70118, USA*
[7]*Department of Physics, Indiana University, Bloomington, Indiana 47408, USA*
[8]*Department of Physics, Shanghai Jiaotong University, Shanghai, 200240, China*
[9]*National Institute of Standards and Technology, Gaithersburg, Maryland 20899, USA*

(Received 23 September 2011; published 7 March 2012)

Using polarized and unpolarized neutron scattering, we show that interstitial Fe in superconducting $Fe_{1+y}Te_{1-x}Se_x$ induces a magnetic Friedel-like oscillation that diffracts at $\mathbf{Q}_\perp = (\frac{1}{2}0)$ and involves >50 neighboring Fe sites. The interstitial $>2\mu_B$ moment is surrounded by compensating ferromagnetic four-spin clusters that may seed double stripe ordering in $Fe_{1+y}Te$. A semimetallic five-band model with $(\frac{1}{2}\,\frac{1}{2})$ Fermi surface nesting and fourfold symmetric superexchange between interstitial Fe and two in-plane nearest neighbors largely accounts for the observed diffraction.

DOI: 10.1103/PhysRevLett.108.107002 PACS numbers: 74.70.Xa, 74.25.Ha

While superconducting $Fe_{1+y}Te_{1-x}Se_x$ shares band structure, Fermi surface [1], and a spin resonance [2] with Fe pnictide superconductors [3–5], the parent magnetic structures are surprisingly different. Figure 1(a) depicts the distinct magnetic unit cells with single striped order for 122 arsenides [$\mathbf{q}_m = (\frac{1}{2}, \frac{1}{2})$] [6] versus double stripes for $Fe_{1+y}Te$ [$\mathbf{q}_m = (\frac{1}{2}, 0)$] [7,8]. In this Letter, we show that short range ordered glassy magnetism at $(\frac{1}{2}, 0)$ in superconducting $Fe_{1+y}Te_{1-x}Se_x$ ($x = 0.38$) arises from magnetic Friedel-like oscillations surrounding interstitial Fe forming what we call a magnetic polaron. A critical role of interstitial iron to stabilize the lamellar structure [9], enhance magnetism [10], and reduce the superconducting volume fraction [11] was previously noted. Our results provide a quantitative microscopic view of the pivotal magnetic polaron.

We used three coaligned $Fe_{1+y}Te_{0.62}Se_{0.38}$ single crystals with total mass ≈ 20 g and $y = 0.01(2)$ determined by energy-dispersive x-ray analysis. Grown by a flux method [11], the samples are tetragonal (space group $P4/nmm$) with low temperature (T) lattice parameters $a = 3.791$ Å and $c = 6.023$ Å. Magnetization and specific heat measurements yielded $T_c = 14.0(2)$ K and a superconducting volume fraction of 92.9(7)% and 83(1)%, respectively [Fig. 5(b)].

Neutron scattering was performed by using the Multi Axis Crystal Spectrometer at National Institute of Standards and Technology Center for Neutron Research [12]. Twenty detection channels permitted mapping of elastic scattering throughout a reciprocal lattice plane [13]. High T measurements ($T = 25$ K) provided background to cancel the dominant elastic nuclear scattering, so the difference data probe magnetic correlations that become static below 25 K. Polarized neutrons were used to establish the magnetic origin and polarization of the scattering. Spin-polarized ^{3}He gas held in glass cells within a vertical solenoid concentric with the sample rotation axis was used to select the vertical component of neutron spin before and after detected scattering events [14]. The 5 meV flipping ratio was typically 56 and 8.4 for Bragg scattering from Al_2O_3 and $Fe_{1+y}Te_{0.62}Se_{0.38}$, respectively. The corresponding sample depolarization factor of 0.825 was T-independent between 4 and 30 K. A channel mixing correction, obtained from the measured flipping ratio, and transmission correction for time-dependent ^{3}He polarization ($\tau \approx 60$–90 h)—averaging 60 (42) for the non-spin-flip (spin-flip) channel—was applied to T-difference

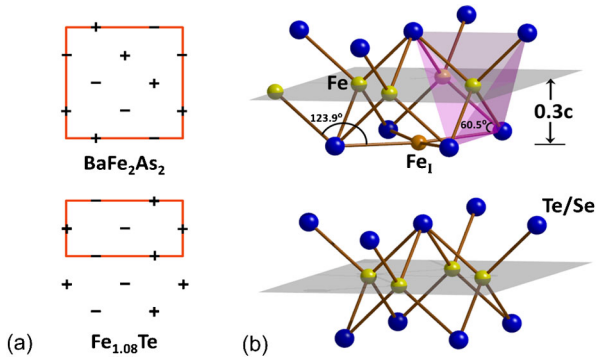

FIG. 1 (color online). (a) Fe-plane magnetic order in the 122 and 11 parent compounds. (b) Half unit cell of $Fe_{1+y}Te_{1-x}Se_x$ showing the location of interstitial Fe in orange (Fe_I).

data. The measurement protocol ensured a less than 5% effect of varying cell transmission on T-difference data. Absolute normalization of the unpolarized scattering cross section was obtained through comparison to acoustic phonon scattering and checked against incoherent elastic scattering from vanadium. The polarized beam configuration was calibrated to the unpolarized configuration through incoherent elastic scattering from the sample.

Figures 2(a) and 2(b) show the wave-vector dependence of the difference between elastic scattering at $T = 1.6$ K and $T = 25$ K. The rodlike nature of scattering in the $(H0L)$ plane [Fig. 2(b)] indicates quasi-2D correlations. Neglecting the interstitial site, $Fe_{1+y}Te_{1-x}Se_x$ has only one Fe site per primitive unit cell. The wave-vector dependence of magnetic neutron scattering associated with the periodic structure therefore must repeat in each Brillouin zone. This implies—modulo the magnetic form factor and polarization factor—that the intensity for $L = \pm\frac{3}{2}$ should match that at $L = \pm\frac{1}{2}$. A possible explanation for the reduced intensity at $L = \pm\frac{3}{2}$ [Fig. 2(b)] is an uniaxial spin configuration $\|\mathbf{c}$, which would imply that magnetic scattering would be exclusively non-spin-flip when neutron polarization $\mathbf{P}\|\mathbf{c}$ [15,16].

Figure 3 shows energy integrated T-difference scattering versus $\mathbf{Q} = (0.535, k, 0)$ for $\mathbf{P}\|\mathbf{c}$. The peak in the spin-flip channel proves *that* part of the scattering cross section is magnetic. By assuming the non-spin-flip T-difference intensity is also magnetic, the intensity ratio of 0.67(12) between the spin-flip and non-spin-flip channels implies that same ratio between the in- and out-of-plane components of the spin correlation function [16]. This ratio is too large for the corresponding polarization factor to account for the reduced intensity at $L = \pm\frac{3}{2}$. Likewise, in the $(HK0)$ plane the elastic magnetic scattering, which comprises four triangle-shaped features at $(\pm\frac{1}{2}, 0)$ and $(0, \pm\frac{1}{2})$, is strongly suppressed in the adjoining Brillouin zones [Fig. 2(a)].

Because the calculated polarization and form factors for magnetic neutron scattering cannot account for the reduced intensities, we are led to conclude that the real space features that give rise to this scattering do not carry the periodicity of the underlying crystal structure. Fourfold rotation symmetry is, however, observed. These facts suggest the involvement of an aperiodic interstitial site. The interstitial Fe_I site [Fig. 1(b)] is located at the center of the primitive square Fe planar unit cell at roughly the same distance $d = zc$ from the Fe plane as the Te(Se) atoms [$z \approx 0.30(3)$] [17,18].

Because of the so-called phase problem and to take into account other knowledge of the chemical structure, we use

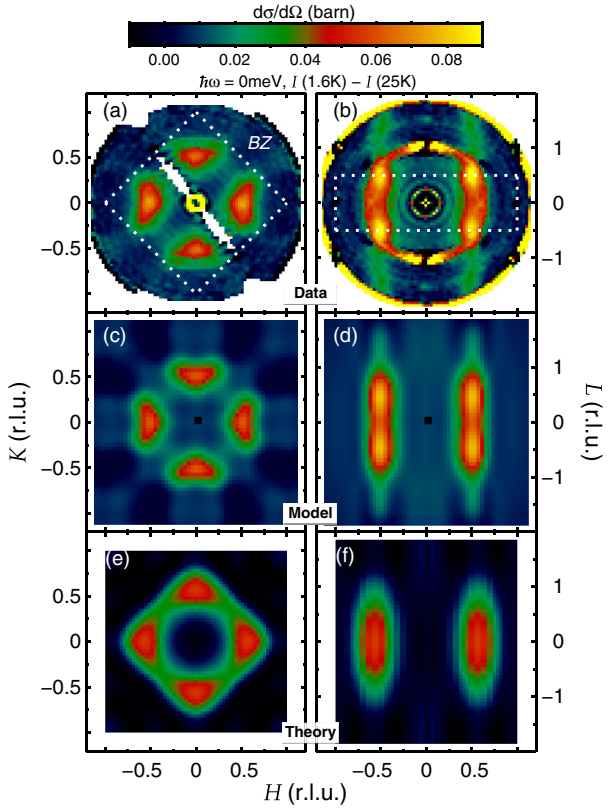

FIG. 2 (color online). (a) Constant $\hbar\omega = 0$ slice showing the difference between neutron scattering intensity I at $T = 1.6$ K and $T = 25$ K in the $(HK0)$ and (b) $(H0L)$ scattering planes with $E_i = E_f = 3.6$ meV. The data were measured with sample rotation about a vertical axis spanning 90°. With the assumption that $I(\mathbf{Q}) = I(-\mathbf{Q})$, the figures show $[I(\mathbf{Q}) + I(-\mathbf{Q})]/2$. Features near the origin, $(0, 0, \pm 1)$ Bragg peaks, and around the perimeter in (b) arise from intense nuclear scattering. (c)–(d) Calculated intensity distribution for a fourfold symmetric spin cluster surrounding interstitial Fe. (e)–(f) Calculated intensity for an interstitial Fe-site exchange coupled to a five d-orbital model.

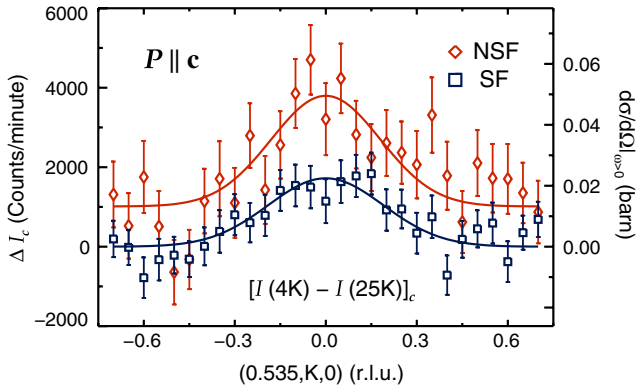

FIG. 3 (color online). Polarized neutron scattering measured along $\mathbf{Q} = (0.535, K, 0)$. $\Delta I_c = [I(4\text{ K}) - I(25\text{ K})]_c$ is the T-difference intensity without energy analysis following ^{3}He cell transmission correction. Red open diamonds are non-spin-flip data, and blue open squares are spin-flip data. The 1.4 mT guide field was perpendicular to $\mathbf{Q}$ and parallel to $\mathbf{c}$. The reduction in the magnitude of the SF + NSF cross section without final energy analysis (≈ 0.06 barn) compared to the energy resolved unpolarized data [≈ 0.07 barn; Fig. 2(a)] is consistent with expectations for frozen spin systems [30]. Here and throughout the Letter, error bars indicate ± 1 standard deviation.

least-squares fitting rather than a direct Fourier transform to obtain the real space spin configuration from the diffuse scattering. The parameters are magnetic dipole moments for the interstitial site and a total of 11 nonequivalent surrounding sites in each of the two planes sandwiching the interstitial. Since there is insufficient information for separate determination of spin configurations in these two planes, the number of free parameters is reduced by forcing identical spin configurations in both planes, allowing them to differ only by an attenuation factor η to account for weaker coupling to the more distant plane. Ordered by distance from the interstitial site, the distinct dipole moments in the near plane are denoted m_n, where $n = 1, 2, 3, \ldots, 11$. The corresponding displacement vectors from the interstitial site are labeled $\mathbf{r}_{nj}$, where j indexes symmetry-related sites. The parameters are inferred by minimizing the least-squared deviation between the corresponding scattering function: $\mathcal{S}(\mathbf{Q}) \propto |m_0 + \sum_{nj} m_n \exp(i\mathbf{Q}\cdot\mathbf{r}_{nj})[1 + \eta \exp(i\mathbf{Q}\cdot\mathbf{c})]|^2$ and the observed wave-vector-dependent T-difference intensity in the $(HK0)$ and $(H0L)$ planes. Here m_0 is the interstitial dipole moment.

The best fit $\mathcal{S}(\mathbf{Q})$ is shown in Figs. 2(c) and 2(d). That we are able to reproduce diffraction throughout the $(HK0)$ and $(H0L)$ planes with a value of $z = 0.23(6)$ consistent with structural data, and $\eta = -0.16(9)$ indicating antiferromagnetic correlation between adjacent planes, confirms interstitial magnetism. The inferred spin configuration is depicted in Fig. 4(a). The interstitial dipole moment is indicated by the central yellow dot, and the surrounding moments are represented by yellow (blue) dots [parallel (antiparallel) with m_0]—their magnitude proportional to the area of the dots. We see that the nearest neighbor (NN) moments are parallel to the interstitial Fe moment. This is consistent with the acute Fe-Te(Se)-Fe_I bond angle [60.5°, Fig. 1(b)], which is expected to yield ferromagnetic (FM) superexchange [19]. Next-nearest neighbors (NNN), on the other hand, are antiparallel to the interstitial moment as expected for the obtuse (123.9°) Fe-Te(Se)-Fe_I bond angle. Comparison to atomic displacement discovered through diffuse x-ray scattering from $Fe_{1+y}Te$ [20] shows FM [antiferromagnetic (AFM)] correlated spins are repelled (attracted), which is consistent with magnetoelastic displacements that enhance magnetic exchange interactions. FM square plaquettes seen along the diagonal direction in Fig. 4(a) are a resilient feature of magnetism in the 11 series that has also been noted in $Fe_{1.1}Te$ [21] and Fe-vacancy ordered $K_yFe_{2-x}Se_2$ [22].

We also adjusted an overall spin space anisotropy parameter resulting in a ratio of 0.81(13) between $\mathcal{S}^{\perp}$ and $\mathcal{S}^{zz}$. Consistency with the polarized beam value of 0.67(12) affirms that the elastic T-difference scattering is magnetic. Absolute normalization of the intensity data further allows extracting $ym_0^2 = 0.22(3)\mu_B^2$. Note that this represents a lower bound on the frozen moment, because this results from a temperature difference measurement. For comparison, the product of the nominal and energy-dispersive x-ray analysis determined interstitial density and the squared free ion dipole moment of Fe^{3+}, $m_0 = 5\mu_B$, consistently yields $ym_0^2 = 0.25\mu_B^2$.

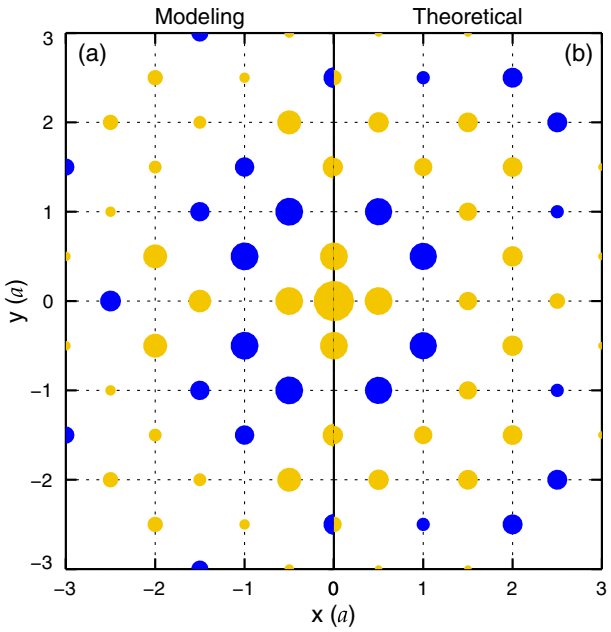

FIG. 4 (color online). Magnetic cluster in nearest neighbor Fe plane surrounding interstitial Fe: (a) inferred from the observed diffuse scattering pattern in Fig. 2 and (b) calculated from a five-band theoretical model. Yellow (blue) moments are parallel (antiparallel) to the interstitial, and the dot areas are proportional to the moment sizes.

The interstitial together with the two nearest neighbors is sufficient to reproduce the major features observed in the $(HK0)$ and the $(H0L)$ scattering planes. The finer details of Fig. 2(c), however, are obtained only when moments beyond reach of direct superexchange interactions are included in $\mathcal{S}(\mathbf{Q})$. These display an oscillatory behavior reminiscent of a Friedel oscillation. For a more rigorous analysis that links the oscillatory magnetism to the Fermi surface structure of itinerant electrons as for the charge density in Friedel oscillations, we use a five-band model with exchange interactions to the two nearest Fe spins. The Hamiltonian consists of three terms:

$$\mathcal{H} = \mathcal{H}_0 + \mathcal{H}_{\text{int}} + \mathcal{H}_{\text{imp}}, \tag{1}$$

where $\mathcal{H}_0$ describes the band structure within the five d-orbital model and $\mathcal{H}_{\text{int}}$ includes the intra- (inter)orbital repulsion U (U'), Hund coupling J_H, and interorbital pair hopping G_2 [23,24]:

$$\mathcal{H}_{\text{int}} = U\sum_{i,\mu}\hat{n}_{i\mu\uparrow}\hat{n}_{i\mu\downarrow} + \frac{U'}{2}\sum_{\substack{i,\mu\neq\nu\\ \sigma,\sigma'}}\hat{n}_{i\mu\sigma}\hat{n}_{i\nu\sigma'} - J_H\sum_{i,\mu\neq\nu}\mathbf{S}_{i\mu}\cdot\mathbf{S}_{i\nu} + \frac{G_2}{2}\sum_{\substack{\mu\neq\nu\\ \sigma\neq\sigma'}} f^{\dagger}_{i\mu\sigma}f^{\dagger}_{i\mu\sigma'}f_{i\nu\sigma'}f_{i\nu\sigma}.$$

Here i and μ are site and orbital indices, respectively. We use a primitive unit cell containing one Fe site with the Brillouin zone indicated in Fig. 2. Wave vectors in this unfolded zone are denoted by dimensionless vectors $\mathbf{k} = \mathbf{Q}a/\sqrt{2}$. We index $\mathbf{k} = k_x\hat{\mathbf{x}} + k_y\hat{\mathbf{y}}$ in a coordinate system rotated by 45° compared to that used for $\mathbf{Q} = H\mathbf{a}^* + K\mathbf{b}^*$ so that $k_x = (H + K)\pi$ and $k_y = (H - K)\pi$. The bare static susceptibility is

$$\chi^0_{\mu\rho,\nu\lambda}(\mathbf{q}) = \int \frac{d\mathbf{k}}{(2\pi)^2} \sum_{\omega_n} G_{\mu\nu}(\mathbf{k} + \mathbf{q}, \omega_n) G_{\lambda\rho}(\mathbf{k}, -\omega_n),$$

where $\omega_n = (2n + 1)\pi T$ and $G_{\mu\nu}(\mathbf{k}, \omega)$ is the orbital Green's function. The nonzero elements of the $5^2 \times 5^2$ interaction matrix are denoted $\hat{V}_{\mu\mu\mu\mu} = U$, $\hat{V}_{\mu\nu\mu\nu} = U'$, $\hat{V}_{\mu\mu\nu\nu} = J_H$, and $\hat{V}_{\mu\nu\nu\mu} = G_2$, where $\mu \neq \nu$. Within the random phase approximation, the full spin susceptibility is $\chi^s(\mathbf{q}) = \frac{1}{2}\sum_{\mu\nu}\chi^{\mathrm{RPA}}_{\mu\mu,\nu\nu}(\mathbf{q})$, where $\chi^{\mathrm{RPA}} = \chi^0(1 - V\chi^0)^{-1}$. We simplify the description of the Fe planes near a magnetic instability by assuming rotational symmetry for interactions, which implies $J_H = G_2$ and $U' = U - J_H - G_2$ [25,26].

$\mathcal{H}_{\mathrm{imp}}$ describes the exchange interaction between the interstitial Fe and neighboring Fe sites:

$$\mathcal{H}_{\mathrm{imp}} = J\mathbf{S} \cdot \sum_{i \in \mathrm{NN}} \mathbf{s}_i + J'\mathbf{S} \cdot \sum_{j \in \mathrm{NNN}} \mathbf{s}_j. \tag{2}$$

Here $J < 0$ ($J' > 0$) is the FM (AFM) exchange constant between the impurity spin and the four NN (eight NNN) spins in the Fe plane. $\mathcal{H}_{\mathrm{imp}}$ is treated as a perturbation to $\mathcal{H}_{\mathrm{int}}$, with the impurity spin fixed. To leading order, we obtain

$$s(\mathbf{k}) = -4\chi^s(\mathbf{k})\Big\{J\cos\Big(\frac{k_x}{2}\Big)\cos\Big(\frac{k_y}{2}\Big) + J'\Big[\cos\Big(\frac{k_x}{2}\Big)\cos\Big(\frac{3k_y}{2}\Big) + \cos\Big(\frac{3k_x}{2}\Big)\cos\Big(\frac{k_y}{2}\Big)\Big]\Big\}. \tag{3}$$

The structure factor, including the contribution of the impurity spin, is $\mathcal{S}(\mathbf{Q}) \propto |1 + s(\mathbf{k})|^2$. While χ^s has nesting peaks at $\mathbf{k} = (\pi, 0)$ [$\mathbf{Q} = (\frac{1}{2}, \frac{1}{2})$] [23,24], these are suppressed by the braces in Eq. (3). The fit to the experimental data gives $U = 0.95(5)$ eV, $J_H = G_2 = 0.05(5)$ eV, $J = -70$ meV, and $J' = 40$ meV. Consistent with the *effective* nature of $\mathcal{H}_{\mathrm{imp}}$, there is a considerable robustness to the fit: The essential features are the FM J versus AFM J' and $0.2|J| < J' < 0.8|J|$. For comparison, the dominant NN and NNN exchange constants in $Fe_{1.05}Te$, with similar Fe-Te-Fe bond angles, are $J = -51(3)$ meV and $J' = 22(4)$ meV, respectively [27].

The calculated structure factor $\mathcal{S}(\mathbf{Q})$ is shown in Figs. 2(e) and 2(f) and the corresponding real space magnetization map in Fig. 4(b). By comparing to the experimental data [Fig. 4(a)], there is reasonable agreement up to the third NN beyond which the theory overestimates the magnitude of induced magnetization and modulation along the $(\frac{1}{2}, \frac{1}{2})$ direction. Possible reasons include lack of orbital specificity to the interaction parameters and effects from neighboring interstitial sites. Indeed, the appearance of nominally elastic diffuse magnetic scattering in our experiment indicates a spin-glass-like state that links interstitials. Further information about associated spin dynamics was recently provided for $Fe_{1.01}Te_{0.72}Se_{0.28}$ [28].

Confirming indications from resistivity measurements [11] and predictions from density functional theory [29], our data show that the interstitial site develops a full local moment. Superexchange interactions further enforce FM plaquettes around impurities with fairly large magnetic moments. Sprinkled at random through the sample, these favor spin configurations where the primitive unit cell carries the dipole moment so that the $(\frac{1}{2}0)$-type double stripe structure emerges as a compromise between the $(\frac{1}{2}\,\frac{1}{2})$ semimetallic nesting instability and FM superexchange interactions. Indeed, this manifests in our impurity band structure calculation [Fig. 2(e)].

We now examine the interplay between interstitial glassy magnetism and superconductivity. Figure 5(a) shows the T dependence of inelastic scattering at $\mathbf{Q} = (\frac{1}{2}, \frac{1}{2})$ which is sensitive to magnetic fluctuations linked to $s_\pm$ superconductivity [2]. The intensity is precipitously suppressed for $T < T_c$ as the gap opens and the spin resonance develops. The elastic scattering at $(\frac{1}{2}, 0)$, on the other hand, grows upon cooling with no apparent anomaly at T_C. Despite the 1% level interstitial concentration, the spatial extent of the associated Friedel oscillation (> 50 neighboring Fe sites, Fig. 4) ensures the majority of the Fe atoms are involved and thus microscopic coexistence with the >80% superconducting volume fraction.

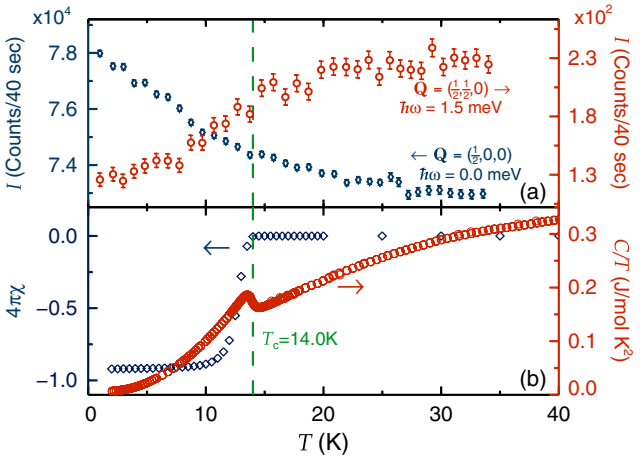

FIG. 5 (color online). (a) T dependence of neutron scattering intensity at $\mathbf{Q} = (\frac{1}{2}, 0, 0)$ and $\hbar\omega = 0.0$ meV (red) and $\mathbf{Q} = (\frac{1}{2}, \frac{1}{2}, 0)$ and $\hbar\omega = 1.5$ meV (blue). (b) dc susceptibility measurement at $\mu_0 H = 3$ mT (blue diamonds) showing diamagnetic screening which yields an upper bound of 92.9(7)% on the superconducting volume fraction. Specific heat data (red circles) from which a volume fraction of 83% is extracted.

The large energy scales ($-J, J' \gg k_B T_c$) that control the interstitial polaron and the different characteristic wave vectors associated with magnetism and superconductivity are surely relevant here. At the same time, previous studies show that interstitial iron does reduce the superconducting volume fraction [11]. These facts suggest that two length scales are involved as in the mixed phase of a type II superconductor: polaron cores accounting for the ~17% normal volume fraction, with Friedel oscillations permeating the superconducting bulk.

We thank Tyrel McQueen for helpful discussions. Work at IQM was supported by DoE, Office of Basic Energy Sciences, Division of Materials Sciences and Engineering under Grant No. DE-FG02-08ER46544. W. B. (Renmin University of China) was supported by NSFC Grant No. 11034012 and 973 Program Grants No. 2012CB921700 and No. 2011CBA00112. Work at Tulane was supported by the NSF under Grant No. DMR-0645305 and the LA-SiGMA program under Grant No. EPS-1003897. This work utilized facilities at NIST supported in part by NSF through DMR-0116585 and DMR-0944772. The development and application of neutron spin filters was supported in part by DoE, Office of Basic Energy Sciences, under Interagency Agreement No. DE-AI02-10-ER46735 and Indiana University Grant No. DE-FG02-03ER46093.

[1] S.-H. Lee, G. Xu, W. Ku, J. S. Wen, C. C. Lee, N. Katayama, Z. J. Xu, S. Ji, Z. W. Lin, G. D. Gu, H.- B. Yang, P. D. Johnson, Z.-H. Pan, T. Valla, M. Fujita, T. J. Sato, S. Chang, K. Yamada, and J. M. Tranquada, Phys. Rev. B **81**, 220502 (2010).

[2] Y. Qiu, W. Bao, Y. Zhao, C. Broholm, V. Stanev, Z. Tesanovic, Y. C. Gasparovic, S. Chang, J. Hu, B. Qian, M. Fang, and Z. Mao, Phys. Rev. Lett. **103**, 067008 (2009).

[3] C. Liu, G. D. Samolyuk, Y. Lee, N. Ni, T. Kondo, A. F. Santander-Syro, S. L. Bud'ko, J. L. McChesney, E. Rotenberg, T. Valla, A. V. Fedorov, P. C. Canfield, B. N. Harmon, and A. Kaminski, Phys. Rev. Lett. **101**, 177005 (2008).

[4] D. J. Singh and M. H. Du, Phys. Rev. Lett. **100**, 237003 (2008).

[5] R. Osborn, S. Rosenkranz, E. A. Goremychkin, and A. D. Christianson, Physica (Amsterdam) **469C**, 498 (2009).

[6] Q. Huang, Y. Qiu, W. Bao, M. A. Green, J. W. Lynn, Y. C. Gasparovic, T. Wu, G. Wu, and X. H. Chen, Phys. Rev. Lett. **101**, 257003 (2008).

[7] T. J. Liu, J. Hu, B. Qian, D. Fobes, Z. Q. Mao, W. Bao, M. Reehuis, S. A. J. Kimber, K. Prokes, S. Matas, D. N. Argyriou, A. Hiess, A. Rotaru, H. Pham, L. Spinu, Y. Qiu, V. Thampy, A. T. Savici, J. A. Rodriguez, and C. Broholm, Nature Mater. **9**, 718 (2010).

[8] W. Bao, Y. Qiu, Q. Huang, M. A. Green, P. Zajdel, M. R. Fitzsimmons, M. Zhernenkov, S. Chang, M. Fang, B. Qian, E. K. Vehstedt, J. Yang, H. M. Pham, L. Spinu, and Z. Q. Mao, Phys. Rev. Lett. **102**, 247001 (2009).

[9] H. Okamoto and L. E. Tanner, Bull. Alloy Phase Diagrams **11**, 371 (1990).

[10] E. E. Rodriguez, C. Stock, P.-Y. Hsieh, N. Butch, J. Paglione, and M. A. Green, Chem. Sci. **2**, 1782 (2011).

[11] T. J. Liu, X. Ke, B. Qian, J. Hu, D. Fobes, E. K. Vehstedt, H. Pham, J. H. Yang, M. H. Fang, L. Spinu, P. Schiffer, Y. Liu, and Z. Q. Mao, Phys. Rev. B **80**, 174509 (2009).

[12] J. A. Rodriguez, D. M. Adler, P. C. Brand, C. Broholm, J. C. Cook, C. Brocker, R. Hammond, Z. Huang, P. Hundertmark, J. W. Lynn, N. C. Maliszewskyj, J. Moyer, J. Orndorff, D. Pierce, T. D. Pike, G. Scharfstein, S. A. Smee, and R. Vilaseca, Meas. Sci. Technol. **19**, 034023 (2008).

[13] The sample was oriented with the b axis vertical for the $(H0L)$ scattering plane and the c axis vertical for the $(HK0)$ plane.

[14] C. B. Fu, T. R. Gentile, G. L. Jones, W. C. Chen, R. Erwin, S. Watson, C. Broholm, J. A. Rodriguez-Rivera, and J. Scherschligt, Physica (Amsterdam) **406B**, 2419 (2011).

[15] For a vertical guide field as in our experimental configuration, i.e., $\mathbf{Q} \perp \boldsymbol{P} || \mathbf{c}$, the non-spin-flip scattering intensity $I^{++} = I_{||}^{\mathrm{mag}} + \frac{1}{3} I_{\mathrm{NSI}} + I_N + B$, and the spin- flip scattering intensity $I^{+-} = I_{\perp}^{\mathrm{mag}} + \frac{2}{3} I_{\mathrm{NSI}} + B$, where $I_{||}^{\mathrm{mag}} (I_{\perp}^{\mathrm{mag}})$ is the component of the magnetic scattering $||(\perp)\mathbf{c}$, and the other terms are I_{NSI} = nuclear spin incoherent scattering intensity, I_N = nuclear scattering intensity (other than I_{NSI}), and B = background [16].

[16] R. M. Moon, T. Riste, and W. C. Koehler, Phys. Rev. **181**, 920 (1969).

[17] R. Viennois, E. Giannini, D. van der Marel, and R. Cerny, J. Solid State Chem. **183**, 769 (2010).

[18] S. Li, C. de la Cruz, Q. Huang, Y. Chen, J. W. Lynn, J. Hu, Y. L. Huang, F. C. Hsu, K. W. Yeh, M. K. Wu, and P. Dai, Phys. Rev. B **79**, 054503 (2009).

[19] J. B. Goodenough, *Magnetism and the Chemical Bond* (Wiley, New York, 1963).

[20] X. Liu, C.-C. Lee, Z. J. Xu, J. S. Wen, G. Gu, W. Ku, J. M. Tranquada, and J. P. Hill, Phys. Rev. B **83**, 184523 (2011).

[21] I. A. Zaliznyak, Z. Xu, J. M. Tranquada, G. Gu, A. M. Tsvelik, and M. B. Stone, Phys. Rev. Lett. **107**, 216403 (2011).

[22] W. Bao, Q.-Z. Huang, G.-F. Chen, M. A. Green, D.-M. Wang, J.-B. He, and Y.-M. Qiu, Chin. Phys. Lett. **28**, 086104 (2011).

[23] K. Kuroki, S. Onari, R. Arita, H. Usui, Y. Tanaka, H. Kontani, and H. Aoki, Phys. Rev. Lett. **101**, 087004 (2008).

[24] V. Cvetkovic and Z. Tesanovic, Phys. Rev. B **80**, 024512 (2009).

[25] A. M. Olés, Phys. Rev. B **28**, 327 (1983).

[26] K. Yada and H. Kontani, J. Phys. Soc. Jpn. **74**, 2161 (2005).

[27] O. J. Lipscombe, G. F. Chen, C. Fang, T. G. Perring, D. L. Abernathy, A. D. Christianson, T. Egami, N. Wang, J. Hu, and P. Dai, Phys. Rev. Lett. **106**, 057004 (2011).

[28] S. Chi, J. A. Rodriguez-Rivera, J. W. Lynn, C. Zhang, D. Phelan, D. K. Singh, R. Paul, and P. Dai, Phys. Rev. B **84**, 214407 (2011).

[29] L. Zhang, D. J. Singh, and M. H. Du, Phys. Rev. B **79**, 012506 (2009).

[30] C. Stock, S. Jonas, C. Broholm, S. Nakatsuji, Y. Nambu, K. Onuma, Y. Maeno, and J.-H. Chung, Phys. Rev. Lett. **105**, 037402 (2010).